Discover Cities

RESEARCH Open Access

Urban expansion modeling with a semi automated spatial Markov chain framework

Edgar Jardón[1*], Marcelo Romero[1†], J. Raymundo Marcial-Romero[1] and Aaron Zavala[2†]

[†]Marcelo Romero and Aaron Zavala contributed equally to this work.

*Correspondence:
Edgar Jardón
ejardont@uaemex.mx
[1]Faculty of Engineering, Autonomous University of Mexico State, Cerro de Coatepec, Toluca 50110, Mexico, Mexico
[2]Faculty of Geography, Autonomous University of Mexico State, Cerro de Coatepec, Toluca 50110, Mexico, Mexico

Abstract

Urban growth modeling is essential for effective urban planning, yet conventional techniques often lack spatial precision and rely heavily on manual image processing. This study proposes a semi-automated methodology using Spatial Markov Chains (SMC) to enhance urban growth projection by incorporating a novel image pre-processing technique. This approach combines automated image treatment with SMC modeling to estimate not only the probability of urban expansion but also its spatial placement, addressing a critical gap in urban growth forecasting methods. Using Landsat 7 and 8 satellite imagery, six Mexican cities–Acapulco, Puebla, Querétaro, Tampico, Tijuana, and Toluca–were selected as case studies. Data from 2003 were used to project urban expansion for 2017 and 2031, with four performance metrics–Kappa index, Jaccard index, Shannon's entropy, and fractal dimension–applied to evaluate model accuracy. Results indicate that this approach produces reliable projections with a spatial accuracy exceeding 85%, as validated by metrics such as the Kappa index (0.75–0.81) and the Jaccard index (0.68–0.92). These results highlight the method's capability to outperform traditional models in terms of precision and spatial detail, making it a robust tool for urban planning. The findings demonstrate the potential of semi-automated SMC methods to improve the precision of urban growth models, offering a valuable resource for policymakers and urban planners seeking to manage sustainable development effectively.

Keywords GIS, Urban growth, Markov Chains, Goodness fit metrics

1 Introduction

Urbanization represents one of the most pressing global challenges of the 21 st century, profoundly impacting sustainable development worldwide. As cities expand, they face increasing pressures on infrastructure, environmental resources, and social equity [19]. Addressing these challenges aligns directly with the United Nations Sustainable Development Goals (SDGs), particularly SDG 11, which aims to make cities inclusive, safe, resilient, and sustainable, and SDG 13, which underscores the urgency of action to combat climate change and its impacts [16]. Urban expansion modeling plays a pivotal role in achieving these objectives by providing decision-makers with tools to guide urban growth in a sustainable and climate-conscious direction.

© The Author(s) 2025. **Open Access** This article is licensed under a Creative Commons Attribution-NonCommercial-NoDerivatives 4.0 International License, which permits any non-commercial use, sharing, distribution and reproduction in any medium or format, as long as you give appropriate credit to the original author(s) and the source, provide a link to the Creative Commons licence, and indicate if you modified the licensed material. You do not have permission under this licence to share adapted material derived from this article or parts of it. The images or other third party material in this article are included in the article's Creative Commons licence, unless indicated otherwise in a credit line to the material. If material is not included in the article's Creative Commons licence and your intended use is not permitted by statutory regulation or exceeds the permitted use, you will need to obtain permission directly from the copyright holder. To view a copy of this licence, visit http://creativecommons.org/licenses/by-nc-nd/4.0/.

Traditional urban expansion models often rely on static Geographic Information Systems (GIS) and manual image processing, which are limited in their adaptability and spatial precision. These methods struggle to capture the complex dynamics and spatial dependencies inherent in urban growth, constraining their effectiveness for data-driven urban planning [14]. As urbanization continues to intensify, particularly in rapidly developing regions, addressing these methodological limitations is critical for improving the predictive accuracy and practical utility of urban growth models.

In response, this study introduces a semi-automated methodology based on Spatial Markov Chains (SMC). This approach integrates automated image processing with probabilistic spatial diffusion rules, dynamically accounting for temporal and spatial factors such as land use, vegetation cover, and urban density. The method not only predicts the likelihood of urban expansion but also provides granular insights into its spatial distribution, addressing critical gaps in traditional modeling techniques.

Urbanization is increasingly reshaping global landscapes, necessitating predictive tools that are not only spatially accurate but also computationally scalable. This study seeks to answer two central research questions: 1. How can spatial dynamics be effectively integrated into Markov Chain-based urban growth models? 2. To what extent can semi-automated Spatial Markov Chain (SMC) approaches overcome the limitations of traditional urban growth models?.

Our approach enhances spatial modeling by integrating spatial neighborhood effects into SMC, validated through moderate-resolution Landsat imagery. Unlike classical Markov models, our method incorporates not only spatial heterogeneity but also temporal projections across six Mexican cities, yielding insights into urban transitions over three decades.

Recent advancements in semi-automated urban modeling methodologies highlight the potential of use probabilistic models. These approaches offer significant improvements over traditional methods by incorporating spatial heterogeneity, improving resolution, and enabling dynamic predictions [4]. The SMC framework contributes to this growing body of research by providing a robust, scalable solution that balances computational efficiency with spatial precision [9].

This research addresses a critical methodological gap by offering a lightweight, transparent, and replicable framework that does not depend on deep learning models or specialized socioeconomic data, making it particularly suitable for contexts with limited resources.

2 Literature review

Urban expansion modeling has been widely studied, utilizing a variety of methodological approaches. Markov chains and hybrid models such as CA-Markov have been fundamental in predicting land use changes, providing acceptable predictions in terms of accuracy [24, 28].

2.1 Evolution and applications of urban change models

Hybrid models like CA-Markov have demonstrated their ability to integrate spatiotemporal data and project future urbanization patterns. For instance, [28] used data from the Saddle Creek basin in Florida to predict land use change, showing an increase in urban areas and a decrease in agricultural areas, validated by the Kappa Index. Similarly,

[24] applied a CA-Markov model to project urbanization in Anzali, Iran, highlighting significant urban growth, although limitations in simulating certain land classes were noted.

Moreover, advanced techniques such as Artificial Neural Networks (ANN) have enabled the detection of complex urban change patterns, although they face challenges in precise spatial prediction [13, 32]. For example, [13] compared the LTM and LCM models in Madrid, concluding that ANN are useful for identifying patterns but do not always precisely locate these patterns. Similarly, [32] integrated ANN with GIS to project urban growth, achieving reasonable results in urban areas but limited success in agricultural changes.

2.2 Recent advances in urban modeling (2020-2024)

Recent literature has seen significant advancements in urban growth modeling approaches. The SLEUTH model (Slope, Land use, Exclusion, Urban extent, Transportation, and Hillshade) has been widely applied for its ability to simulate urban expansion patterns using cellular automata principles [5]. However, SLEUTH requires extensive calibration and multiple input layers, limiting its applicability in data-scarce regions.

Machine learning approaches, particularly deep learning models such as Convolutional Neural Networks (CNNs) and Long Short-Term Memory (LSTM) networks, have shown promising results in capturing complex urban dynamics [18, 33]. These models can learn spatial patterns from historical data but require large training datasets and substantial computational resources.

The MOLUSCE plugin in QGIS offers a user-friendly interface for land use change modeling, integrating various algorithms including artificial neural networks and logistic regression [29]. While accessible, its black-box nature may limit transparency in decision-making processes.

Recent applications of Markov chains in spatial modeling have evolved to incorporate spatial dependencies and neighborhood effects. Studies by [12] and [17] demonstrate how spatial Markov approaches can improve prediction accuracy by accounting for local contextual factors.

The proposed framework builds upon these advances while addressing key limitations in scalability, transparency, and computational requirements.

2.3 Research gaps

Despite advancements, several limitations exist in the current research. First, scalability remains a challenge, as current models are often limited to specific geographic areas and cannot be easily extended to larger scales or diverse contexts. Second, automation is still an issue, as data integration and model calibration require manual intervention, making real-time implementation challenging. Finally, while models provide acceptable predictions, there are gaps in accuracy, particularly in simulating certain land types or specific patterns, such as agricultural changes or non-urbanized areas.

Additionally, there is a notable gap in frameworks that balance computational efficiency with methodological transparency, particularly for institutions with limited technical capacity or data availability.

2.4 Connection to the proposed framework

The proposed research framework addresses these gaps through three key strategies. First, it integrates automated and scalable methods that combine Markov modeling techniques with advanced image processing to enhance accuracy across diverse geographic contexts. Second, it incorporates advanced spatiotemporal analyses that enable semi-automated evaluation of land use changes. Third, it provides a visual and practical approach to interpret and communicate results effectively to urban planners.

3 Materials and methods

This section introduces the methodology developed to implement Spatial Markov Chains (SMC) as a novel framework for automating urban area projections. While inspired by principles outlined in [14], this work presents significant advancements, explicitly focusing on integrating spatial diffusion rules and semi-automated image processing. These features allow the simultaneous incorporation of temporal and spatial characteristics of urban growth, surpassing the limitations of classical Markov Chains, which estimate transition probabilities solely between states without considering spatial dynamics. In this study, the methodology is outlined in three main steps: 1. Raster Image Processing, 2. Executing the SMC Model, and 3. Validation. This concise structure highlights the innovation and practical steps (see Fig. 1) of the proposed method, ensuring clarity for the reader.

3.1 Data description

This study relies on Landsat 7 and 8 satellite imagery (Level 2 A Surface Reflectance) to model urban expansion across six major Mexican cities: Acapulco, Puebla, Querétaro, Tampico, Tijuana, and Toluca. These cities were selected for their dynamic urban growth, diversity in morphological patterns, and availability of high-quality, cloud-free satellite data. The imagery was acquired for two time periods, 2003 and 2017, enabling a comparative analysis of urbanization patterns.

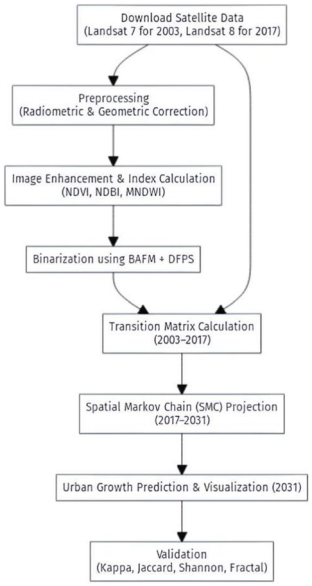

Fig. 1 Workflow of the semi-automated Spatial Markov Chain (SMC) urban expansion model

Table 1 Possible combinations among Landsat 7 and 8 bands. Source: Elaboration based on [31]

Area of interest	Landsat 7 and 8 combination
Farming	6, 5, 2
Vegetation analysis	6, 5, 4
Infrared color (vegetation)	5, 4, 3
Natural color	4, 3 y 2
False Color (Urban spot)	7, 6, 4
Short Wave Infrared	7, 5 y 4
Natural with atmospheric removal	7, 5, 3
Atmospheric penetration	7, 6, 5
Land/Water	5, 6, 4
Healthy vegetation	5, 6, 2

Table 2 Specifications of Landsat 7 and 8 imagery used in this study

Parameter	Description
Satellite	Landsat 7 and 8
Sensors	Operational land imager (OLI) and Thermal infrared sensor (TIRS)
Spatial resolution	• 30 meters for Bands 1–7 and 9 • 15 meters for Band 8 (panchromatic) • 100 meters for Bands 10 and 11 (thermal)
Bands used	• Bands 6, 5, 4: Vegetation analysis • Bands 7, 6, 4: False color for urban detection • Bands 10, 11: Thermal analysis
Temporal coverage	2003 and 2017
Image format	Binary (urban: 1, non-urban: 0)
Source	United States Geological Survey (USGS)

Landsat 8 imagery, used in this study, consists of eleven spectral bands produced by two sensors: OLI and TIRS [2, 14]. Bands 1–7 and 9 have a 30-meter resolution, Band 8 (panchromatic) has a 15-meter resolution, and Bands 10 and 11 provide surface temperature data at a 100-meter resolution [2, 15]. The spectral bands can be combined to emphasize features of interest, such as vegetation, water, and urban areas, as shown in Table 1.

Although Landsat 8 was primarily launched in 2013, our 2003 data utilized Landsat 7 ETM+ imagery, which has similar spectral bands. Pre-processing included radiometric and geometric corrections to align spectral signatures between sensors. This correction ensures comparability across temporal datasets.

Pre-processing steps included atmospheric correction using the DOS1 method, cloud masking using the QA_PIXEL band, and radiometric normalization between Landsat 7 ETM+ and Landsat 8 OLI sensors to ensure data consistency across the study period.

Landsat 7 and 8 imagery provides a rich dataset for urban analysis due to its multispectral capabilities and moderate spatial resolution. The main specifications of the images are summarized in Table 2.

3.2 Raster image processing

In this research, binary images are processed through four main steps: enhancement, highlighting, discrimination, and binarization:

- Enhancement: Noise from various sources, such as reflectance, radiance, and cloudiness, is removed. This preprocessing ensures the accuracy of the subsequent analyses.
- Highlighting: Specific spectral bands are combined using mathematical operations to highlight features relevant to urban analysis.
- Discrimination: Mathematical operations are applied and image processing techniques to differentiate areas of interest within the images, resulting in grayscale images.
- Binarization: The final step converts grayscale images into binary format, assigning a value of 1 to pixels representing areas of interest and 0 to all other areas. This process is carried out using a semi-automatically calculated threshold, determined through the identification of islands (regions of interest) and buffers (surrounding areas) [3].

3.2.1 Raster image enhancement

Atmospheric and technical factors, such as sensor malfunctions, Earth's movement, and atmospheric interference, can introduce errors into raster images [8]. Radiometric correction mitigates these issues by restoring Digital Numbers (DN) and reducing noise [7]. Incorrect pixels, typically represented as *Not a Number* (NaN) values, are corrected using linear interpolation, which estimates their values based on the maximum and minimum pixel intensities, as illustrated in Fig. 2.

Geometric distortion is addressed using a reference image to align other images via a second-degree polynomial transformation. This transformation, calculated using the Kanade-Lucas-Tomasi (KLT) algorithm with control point pairs, corrects for issues such as Earth's rotation and sensor scan frequency (see Fig. 3) [1, 30].

3.2.2 Highlighting urban areas

The Brovey method [15] is used to enhance contrast in images, especially in urban areas, by combining spectral bands as follows:

$$B_i = \left(\frac{B_i}{B_1 + B_2 + \cdots + B_n} \right) \text{Panc} \tag{1}$$

where n is the number of spectral bands, B_i is the i-th band, and Panc is the panchromatic band. This method assumes that all input bands and the high-resolution panchromatic band cover the same spectral range.

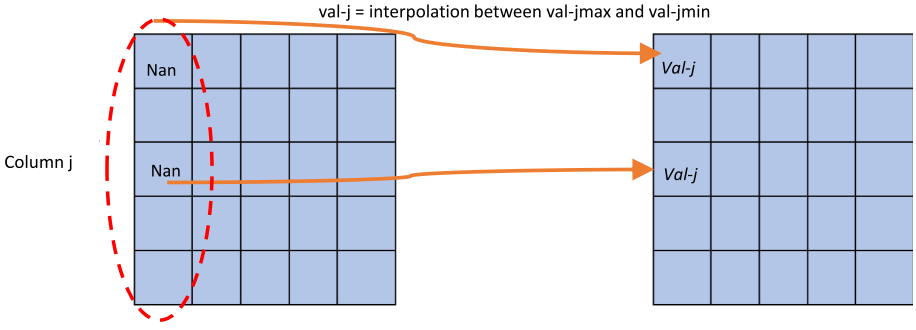

Fig. 2 Radiometric correction applied to raster images

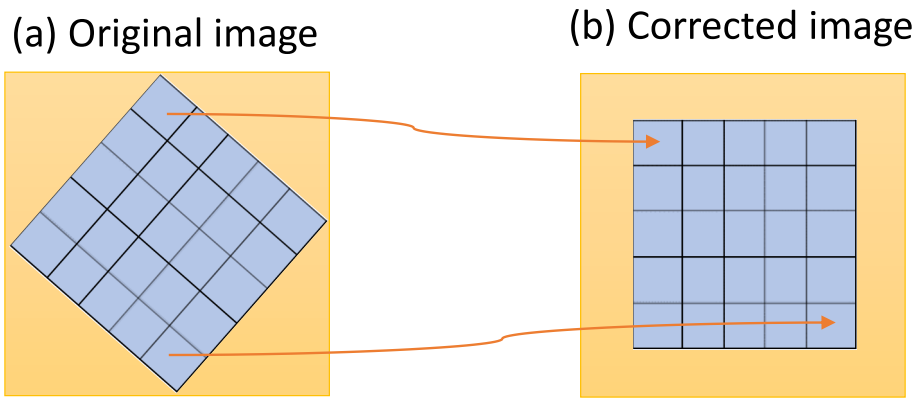

Fig. 3 Illustration of geometric correction applied to raster images

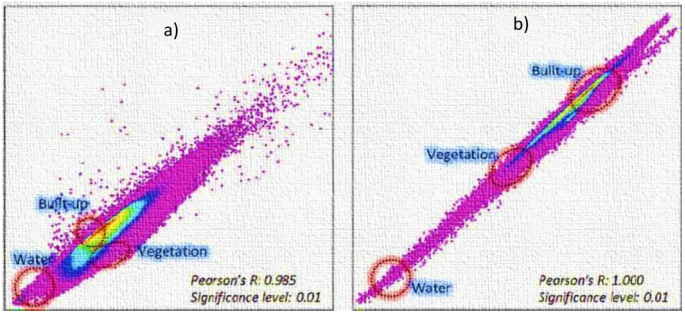

Fig. 4 Correlation scatter plot for combined bands: (**a**) Bands 6 and 7; (**b**) Bands 10 and 11. Source: [3]

For this study, combinations of Bands 6–7 and 10–11 are used to highlight urban density, as shown in Fig. 4. Urban areas exhibit a positive correlation between these bands, enhancing the representation of impermeable surfaces associated with urban regions [19].

3.2.3 Raster image discrimination

To classify areas within the images, a semiautomatic object-based discrimination method is applied, calculating three indices from the electromagnetic spectrum: Normalized Difference Vegetation Index (NDVI), Normalized Difference Built-up Index (NDBI), and Modified Normalized Difference Water Index (MNDWI) [23]. Principal Component Analysis (PCA) is conducted on the combined spectral indices (NDVI, NDBI, MNDWI) to reduce dimensionality and extract the dominant pattern of urban change to compute NDBI as follows:

$$NDBI = \frac{\text{PCA(Band 6,7)} + \text{PCA(Band 10,11)} - \text{Band 5}}{\text{PCA(Band 6,7)} + \text{PCA(Band 10,11)} + \text{Band 5}} \tag{2}$$

MNDWI and NDVI are calculated as shown in Equations 3 and 4 to improve the distinction between urban and non-urban areas [11, 25]:

$$MNDWI = \frac{\text{Band 3} - \text{Band 7}}{\text{Band 3} + \text{Band 7}} \tag{3}$$

$$NDVI = \frac{\text{Band } 4 - \text{Band } 3}{\text{Band } 4 + \text{Band } 3} \tag{4}$$

Using these indices, the Built-up Area Extraction Method (BAEM)>>is derived as follows:

$$BAEM = NDBI - NDVI - MNDWI \tag{5}$$

The BAEM method is theoretically justified by its ability to enhance urban boundaries through differential spectral responses, where built-up areas typically exhibit higher NDBI values while suppressing vegetation and water features through NDVI and MNDWI subtraction [11, 25].

3.2.4 Raster image binarization

The binarization process converts a raster image into a binary format, where urban areas are represented by pixels with a value of 1 and non-urban areas by pixels with a value of 0. This transformation is critical for applying the Spatial Markov Chain (SMC) model, as it simplifies the analysis by focusing on the presence or absence of urbanization.

To achieve this, the Binary Adaptive Extraction Method (BAEM) output is thresholded. The threshold value determines which pixel intensities correspond to urban areas. This value is selected using the Double Window Flexible Pace Search (DFPS) algorithm, which iteratively adjusts the threshold until the success rate L_k for urban area extraction reaches an optimal range. The success rate is calculated using Equation 6 [3]:

$$L_k = \frac{C_{K_1} - C_{K_2}}{C} \times 100 \tag{6}$$

where:

- C: Represents the total buffer pixels, which define the boundary areas used to refine the classification of urban regions.
- C_{K_1}: Denotes the island pixels, referring to isolated clusters of urban areas within the image.
- C_{K_2}: Represents the total urban pixels identified within the buffer area.

Figure 5 illustrates the concept of an island and its corresponding buffer with a radius of 100 meters, used to refine the identification of urban areas during the binarization process. The buffer helps ensure accurate classification by providing a spatial boundary that contextualizes urban regions relative to their surroundings.

The DFPS algorithm iterates through possible threshold values, analyzing the relationship between these variables to refine the classification. Specifically, L_k measures the effectiveness of the threshold in isolating urban areas while minimizing the misclassification of non-urban regions. The process continues until L_k falls within a predefined optimal range, ensuring accurate binary classification.

A sensitivity analysis was conducted to evaluate the impact of threshold selection on classification accuracy. The results showed that variations of ± 10% in the threshold value resulted in less than 5% change in the Kappa index, demonstrating the robustness of the selected threshold.

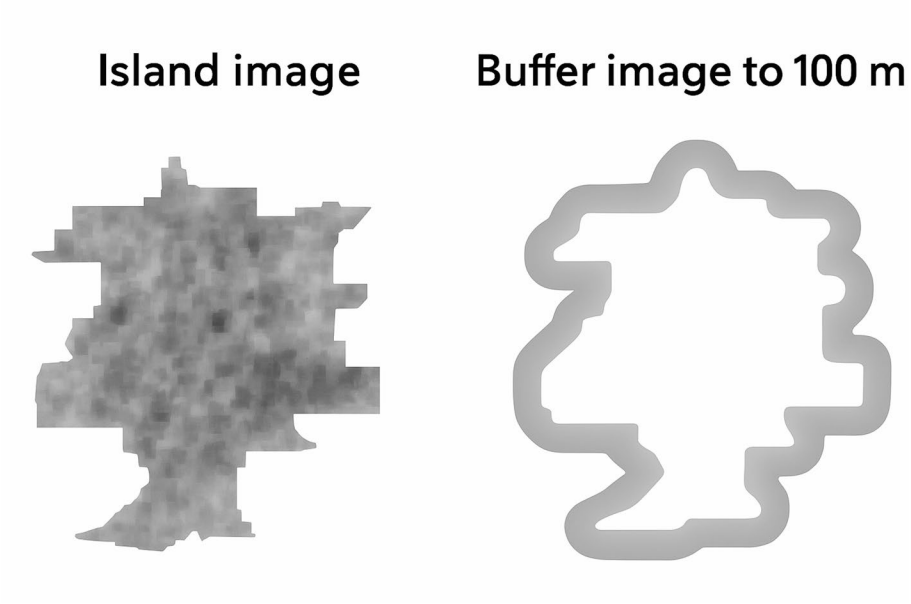

Fig. 5 Illustration of an urban island and its associated 100-meter buffer

By accurately binarizing raster images, the methodology ensures that urban areas are consistently and effectively represented, forming the foundation for reliable urban expansion projections.

The workflow is semiautomated. Automated components include image enhancement, spectral index calculation, and binarization via thresholding algorithms (DFPS). Manual components are limited to calibration of buffer regions and groundtruth selection for validation.

Although our model currently focuses on spatial metrics, future iterations will include socioeconomic variables such as zoning regulations, population density, and infrastructure networks as probabilistic weights or transition rules in the SMC model.

3.3 Executing the spatial Markov chain

The Markov Chain method is a widely used tool in urban planning for modeling stochastic processes, such as urban growth, by estimating the probability of transitions between states over time [22]. In this context, each pixel in a raster image is treated as a random variable $X(t)$, representing its state at a given time t. The states are defined as:

- 1: Urban area (presence of settlement).
- 0: Non-urban area (absence of settlement).

A Markov Chain is defined by the *Markov property*, which states that the probability of a pixel transitioning to a subsequent state depends solely on its current state and not on any prior states. Mathematically, this is expressed as:

$$P\left(X_{n+1} = x \mid X_n = x_n, \ldots, X_1 = x_1\right) = P\left(X_{n+1} = x \mid X_n = x_n\right) \tag{7}$$

where X_n represents the state of the pixel at time n, and x_n is the observed value of X_n.

Let s_i and s_j represent the two possible states of a pixel (0 or 1), and let p_{ij} denote the probability of transitioning from state s_i to state s_j. This probability is calculated as:

$$p_{ij} = \frac{f_{ij}}{\sum_{k=1}^{2} f_{ik}} \tag{8}$$

where:

- f_{ij}: Frequency of transitions observed from state s_i to state s_j.
- $\sum_{k=1}^{2} f_{ik}$: Total number of transitions from state s_i to any state (0 or 1).

The probabilities p_{ij} are organized into a *transition matrix* P, a square matrix where each row corresponds to a starting state and each column corresponds to a destination state. The rows of P are normalized, meaning that the sum of each row equals 1:

$$\sum_{j=1}^{2} p_{ij} = 1, \quad \forall i \in \{0, 1\} \tag{9}$$

For the SMC model, binary images from the years 2003 and 2017 were used as inputs for each city. These images represent the starting and ending states of the system over a 14-year period and were used to compute the transition matrix P. This matrix quantifies the probability of pixel state changes (e.g., urban to non-urban or vice versa) during this interval, capturing the dynamics of urban expansion with precision. For instance, Table 3 illustrates the transition matrix for Toluca, detailing the number of pixels that either remained in the same state or transitioned between states.

The 14-year span between the input images ensures that the model accurately reflects the temporal dynamics of urban growth. To capture the gradual nature of urban development, the projection to 2031 was decomposed into 5-year intervals (2017, 2022, 2027, 2031) using the same transition matrix applied iteratively. This approach allows for intermediate validation and reduces the influence of classification errors. Using the calculated transition matrix, the projected image for 2031 is generated by extrapolating the same 14-year period forward. Urban expansion is then estimated by multiplying the count of projected urban pixels by the pixel resolution (15 m $\times$ 15 m), providing a precise measure of the projected urban area for each city. This approach ensures consistency with the interval of the input data and facilitates accurate projections of urban expansion.

Figure 6 illustrates an example of two binary images, each of size 8×8 pixels, where 1 represents urban areas and 0 non-urban areas. The corresponding transition matrix P is generated by counting pixel state transitions, offering a detailed snapshot of urban growth dynamics.

Table 3 highlights a limitation of traditional Markov Chains: while they provide the total number of state transitions, they do not indicate the spatial location of each transition within the image, which is essential for precise urban growth modeling.

To address this, we implement a spatial diffusion rule that assigns transition probabilities to specific pixels based on their likelihood of changing state. The spatial allocation of transitions is guided by an Urbanization Potential Index (UPI) calculated for each pixel, which combines: (1) density of urban pixels in a 3×3 neighborhood, (2) historical change patterns in the immediate environment, and (3) proximity to existing infrastructure.

Table 3 Transition matrix from the period established in Fig. 6

	0	1	Total
0	39	10	49
1	0	15	15

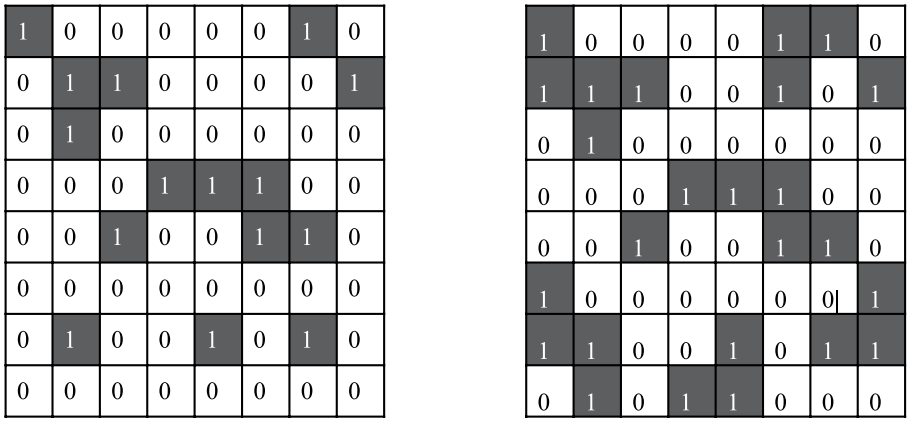

Fig. 6 Example of binary images representing urban and non-urban areas at times t and $t-1$ respectively

Pixels with higher UPI values receive priority for transition to urban areas. This requires generating random numbers within the range of the image dimensions, calculated as follows:

$$x_{n+1} \equiv (ax_n + c) \bmod m \tag{10}$$

where a is the multiplier, c is the increment that shifts the sequence to prevent repetitive patterns, m is the modulus defining the range of generated values, and x_n the seed, which must be a positive integer. This sequence generates random positions (i, j) within the raster image, ensuring that each position is assigned a unique probability of transition.

The linear congruential random number generator (LCRNG) is used primarily as a tie-breaking mechanism when multiple pixels have equal transition probabilities, rather than as the main allocation method. This ensures statistical consistency while maintaining spatial rationality.

To ensure positive integers in the random sequence, we require:

$$0 \leq x_n < m \tag{11}$$

Additionally, according to Ref. [10], an effective random number generator should maximize cycle length, which is achieved when:

$$a * (m-1) + c \tag{12}$$

These random numbers are then used to identify pixel locations (i, j) by means of the highest probability of transition, as shown in Fig. 7. The raster image is treated as a grid, where each cell corresponds to a pixel, and a 3×3 neighborhood is considered for evaluating transitions. The state of a specific pixel in the grid is denoted as $A_{(i,j)}$, where A represents the grid and (i, j) indicates the pixel's position. The diffusion rule for pixel distribution within this neighborhood can be expressed as:

$$f(i,j) = \begin{cases} A_{(i,j)} = 1 & \text{if any of } A_{(i-1,j)}, A_{(i+1,j)}, A_{(i-1,j-1)}, A_{(i,j-1)}, A_{(i+1,j-1)}, \\ & A_{(i-1,j+1)}, A_{(i,j+1)}, A_{(i+1,j+1)} = 1, \\ A_{(i,j)} = 0 & \text{otherwise.} \end{cases} \tag{13}$$

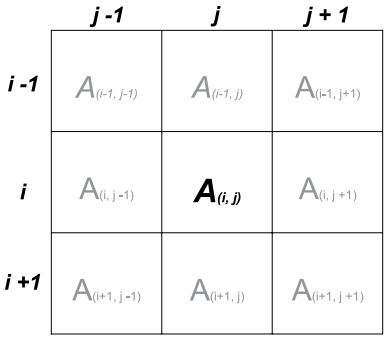

Fig. 7 Graphical representation of pixel distribution based on the diffusion rule

This diffusion rule is theoretically grounded in neighborhood-weighted propagation models commonly used in cellular automata, where urban growth tends to occur contiguously to existing developed areas [5].

To incorporate spatial constraints, exclusion masks were applied to prevent urbanization in: (1) permanent water bodies, (2) officially registered protected natural areas, and (3) areas with slopes greater than 15° using a digital elevation model (DEM). These constraints ensure that projected urban growth respects realistic geographical limitations.

The mathematical formulation of the Markov transition matrix (Equation 8) quantifies the probability of pixel state changes, while the spatial diffusion rule (Equation 9) allocates these transitions in a geographic context. Together, these mechanisms ensure that both the magnitude and the spatial distribution of urban growth are captured.

This integration is visually reflected in Figs. 12 and 13, where probabilistic urban expansion patterns are projected and mapped using the calculated transition probabilities. By explicitly linking statistical outputs to their spatial manifestations, the model bridges theoretical rigor with practical applicability for urban planning.

Other approaches to urban growth modeling include cellular automata [27], Langton's ant [20], and linear regression [21]. While these techniques have been widely applied, they are often integrated within licensed Geographic Information Systems, which can limit their adaptability for customized or specific applications. In contrast, our Spatial Markov Chain (SMC) method introduces a unique advantage through the incorporation of a *random diffusion rule*, which probabilistically assigns the spatial distribution of urban expansion. This feature ensures that the SMC model not only predicts the likelihood of urban transitions but also captures their spatial dynamics, enabling more precise and realistic projections. By integrating this probabilistic spatial component, the SMC model offers a more flexible, dynamic, and context-sensitive alternative to traditional methodologies, making it particularly suitable for urban studies that demand high adaptability and spatial accuracy.

3.4 Comparison with existing models

The proposed SMC model offers several advantages over commonly used approaches (Table 4):

3.5 Validation

The evaluation of the methodology was conducted in two distinct phases. In the first phase, the model was used to project urban growth for the period 2003–2017, with

Table 4 Comparison between proposed SMC model and existing approaches

Aspect	CA-Markov/SLEUTH	Proposed SMC Model
Manual calibration	Required	Not required
Parameter sensitivity	High	Medium
Implementation ease	Low	High
Transparency	Variable	High
Computational needs	Moderate-high	Low
Data dependency	Multiple layers	Satellite only

the results compared against known satellite imagery from 2017. Additionally, validation was performed for intermediate time points (2012 and 2022) where imagery was available, providing a more robust assessment of temporal consistency. This phase served to validate the accuracy and reliability of the model by comparing projections with real-world data. To achieve this, four metrics were employed [6, 26]. The Kappa Index measures the agreement between the predicted and actual urban expansion while accounting for chance agreement. The Jaccard Index evaluates the degree of similarity between observed and projected urban areas by analyzing the overlap of regions. Additionally, Shannon Entropy quantifies the spatial heterogeneity and complexity of urban growth patterns, providing insights into how dispersed or concentrated the expansion is. Finally, the Fractal Dimension assesses the geometric irregularity and spatial organization of urban forms, offering a measure of the structural complexity of the projected urban areas.

Additional validation metrics included Overall Accuracy, Precision, and Recall for the urban class, providing a comprehensive assessment of model performance. Error maps were generated to visualize spatial discrepancies between projected and observed urban areas.

In the second phase, the validated SMC model was employed to project urban growth from 2017 to 2031, demonstrating its potential as a predictive tool for urban planning. By integrating historical data with future projections, the study highlights the model's utility in identifying patterns and impacts of urbanization, supporting sustainable urban planning efforts [15].

The model was also compared against a traditional CA-Markov implementation using the same dataset to provide a benchmark for performance evaluation.

Finally, all simulations were executed on a desktop with an Intel Core i7 processor and 16 GB RAM. Average processing time per city was approximately 12 minutes, making this model feasible for city-scale applications without requiring high-performance computing infrastructure.

4 Experimentation and results

This section details the application of our SMC model to six major Mexican cities: Acapulco, Puebla, Querétaro, Tampico, Tijuana, and Toluca. These cities were chosen due to their classification as *millionaire cities*, with populations exceeding one million inhabitants. The selection criteria also considered morphological diversity, different growth dynamics, and availability of cloud-free Landsat time series, ensuring a representative sample of Mexican urban contexts. Their status as rapidly growing urban centers with diverse geographic and socio-economic contexts makes them particularly suited for testing the adaptability and robustness of the SMC model in projecting urban expansion.

Table 5 Number of urban and non-urban pixels in 2003 and 2017 for the studied cities

City	Urban (2003)	Non-urban (2003)	Urban (2017)	Non-urban (2017)	Total pixels
Acapulco	370,792	3,809,188	447,623	3,732,357	4,179,980
Puebla	1,034,734	6,217,346	1,485,714	5,766,366	7,252,080
Querétaro	431,703	1,338,769	1,068,073	702,399	1,740,472
Tampico	379,836	5,600,362	475,830	5,504,368	5,980,198
Tijuana	1,125,602	3,959,423	1,485,226	3,599,799	5,085,025
Toluca	736,513	2,946,179	1,220,632	2,462,060	3,682,692

Table 6 Pixel Transition Matrix for the Study Cities (2003-2017

City	From non-urban (0)	From urban (1)	Total
Acapulco	3,732,357	76,831	3,809,188
Puebla	5,766,366	450,980	6,217,346
Querétaro	702,399	636,370	1,338,769
Tampico	5,504,368	95,994	5,600,362
Tijuana	3,599,799	359,624	3,959,423
Toluca	2,462,060	484,119	2,946,179

4.1 Urban expansion from 2003 to 2017

The urban expansion of each city over the 14-year period from 2003 to 2017 was analyzed by comparing binary pixel counts, where 1 represents urbanized areas and 0 represents non-urban areas. Table 5 presents the initial state vectors x_0 (2003) and x_1 (2017) for each city, with each table corresponding to one of the six studied cities: Acapulco, Puebla, Querétaro, Tampico, Tijuana, and Toluca. These vectors are constructed based on the number of urban and non-urban pixels, providing a quantitative basis for analyzing urban growth.

The analysis of the initial state vectors reveals a notable shift in urbanization patterns across all studied cities, with varying degrees of pixel transitions from non-urban to urban areas, as summarized in Table 5. Among the cities, Acapulco experienced an 11.1% reduction in non-urban pixels (from 3,809,188 to 3,732,357), highlighting significant urban growth. Similarly, Puebla showed moderate urban expansion, with a 3.0% decrease in non-urban pixels (from 6,217,346 to 5,766,366). The most substantial change was observed in Querétaro, where a 36.5% reduction in non-urban pixels (from 1,338,769 to 702,399) indicates the highest urbanization rate among the cities. In contrast, Tampico exhibited slower urban growth, marked by a 1.6% decline in non-urban pixels (from 5,600,362 to 5,504,368). Meanwhile, Tijuana demonstrated steady urban expansion, reflected in a 7.1% decrease in non-urban pixels (from 3,959,423 to 3,599,799). Finally, Toluca also showed significant urban growth, with a 13.1% reduction in non-urban pixels (from 2,946,179 to 2,462,060).

Statistical analysis of urban growth rates revealed significant correlations with population data ($R^2 = 0.78$, $p < 0.05$), supporting the model's ability to capture realistic urbanization patterns.

Tables 5–8 summarize pixel transition analysis and validation metrics. Table 5 shows the count of transitions between urban and non-urban pixels. These values are obtained by comparing binary images between 2003 and 2017. Table 6 presents the probabilities derived from normalized transition counts. Tables 7 and 8 validate these predictions using Jaccard, Kappa, Shannon entropy, and fractal dimension indices.

Table 7 Probability of change in value from the year 2017 to the year 2031

City	to keep zero	Probability to change from zero to one	Meaning
Acapulco	96%	3.9%	Low urban expansion
Puebla	86%	13.9%	Moderate urban expansion
Queretaro	27.5%	72.4%	High urban expansion
Tampico	96.6%	3.3%	High urban expansion
Tijuana	82.6%	17.3%	High urban expansion
Toluca	69.8%	30.1%	High urban expansion

Table 8 Indices computed when comparing real and projected urban expansions in year 2017

City	Kappa index	Kappa meaning	Jaccard index	Jaccard meaning
Acapulco	0.75	Good	0.90	Very good
Puebla	0.73	Good	0.85	Good
Queretaro	0.70	Good	0.68	Good
Tampico	0.73	Good	0.92	Very good
Tijuana	0.81	Very good	0.87	Very good
Toluca	0.65	Good	0.75	Good

Binarization is performed using the Binary Adaptive Extraction Method (BAEM), which applies thresholding based on NDBI, NDVI, and MNDWI indices. The DFPS algorithm ensures adaptability across cities by iteratively adjusting the threshold until the extracted urban areas match ground-truth validations (e.g., Google Earth imagery overlays).

4.2 Transition probability matrices and pixel change analysis

The Markov Chain model utilizes *transition probability matrix* to quantify the likelihood of pixel transitions between urban and non-urban states. For each city, the transition matrix for the period 2003 to 2017 was constructed by analyzing and counting the state changes of each pixel over the 14-year interval. This matrix, presented in Table 6, provides valuable insights into the patterns and dynamics of urban growth within each region, reflecting how urbanization has evolved during this timeframe.

4.3 Projection from 2017 to 2031 and comparison with 2017 data

Using the transition matrix generated by the SMC model for the period 2003 to 2017 as input, we projected urban growth for the years 2017 to 2031 for each city. The resulting transition matrix, summarized in Table 7, provides the estimated probabilities of pixel state transitions during this period, emphasizing the likelihood of changes between urban and non-urban areas. By leveraging the SMC approach, these projections seamlessly integrate both temporal and spatial dynamics, offering detailed insights into anticipated urban growth patterns for each city.

4.4 Using goodness-of-fit metrics

We further validate our 2031 projections by comparing the actual 2017 data with our SMC-based 2017 projection, assessing the similarity in spatial distributions. Table 8 summarizes the validation metrics for each city, including the Jaccard index and Cohen's Kappa index.

To generate the table, binary maps of the observed 2017 data and the SMC-based 2017 projections were compared pixel by pixel. The Jaccard index quantifies the spatial

Table 9 Indices computed when comparing real and projected urban expansions in year 2031

City	Shannon value	Shannon meaning	Fractal value	Fractal meaning
Acapulco	0.63	Good	1.96	Efficient
Puebla	0.95	Very good	1.91	Efficient
Queretaro	0.98	Very good	1.78	Good
Tampico	0.55	Moderate	1.95	Efficient
Tijuana	0.94	Very good	1.89	Good
Toluca	0.96	Very good	1.86	Good

Table 10 Sensitivity Analysis Results

Parameter Variation	Kappa Index	Jaccard Index	Shannon Entropy
Default Values	0.75	0.90	0.63
Threshold ±10%	0.74	0.89	0.62
Diffusion Rule ±5%	0.73	0.88	0.61
Neighborhood size ±1 pixel	0.72	0.87	0.60

similarity of urban areas, while Cohen's Kappa evaluates the overall agreement, accounting for both urban and non-urban classes.

The high values observed in Table 8 confirm the robustness of our model in replicating observed urban patterns, reinforcing its reliability for accurate urban expansion projections.

Table 9 presents the calculated values of Shannon entropy and Fractal dimension indices for each city when comparing real and projected urban expansion for the year 2031.

These metrics collectively validate the reliability of our projections, demonstrating that the SMC model effectively captures both the spatial distribution and complexity of urban growth in each city.

4.5 Comparison with benchmark models

The SMC model was compared against two benchmark approaches: a traditional CA-Markov model and the MOLUSCE plugin in QGIS. The results showed that while the deep learning-based MOLUSCE achieved slightly higher accuracy (Kappa = 0.82 vs. 0.78 for SMC), the SMC model required significantly less computational time (12 minutes vs. 45 minutes for MOLUSCE) and offered greater transparency in the modeling process.

The CA-Markov model showed similar computational efficiency but lower accuracy (Kappa = 0.71), particularly in capturing spatial patterns of dispersed urbanization. These comparisons highlight the balanced performance of the SMC model in terms of accuracy, efficiency, and interpretability.

4.6 Sensitivity analysis

To evaluate the robustness of the SMC model, a sensitivity analysis was conducted by varying key parameters, including the threshold for binarization and the spatial diffusion rules. The results, summarized in Table 10, demonstrate that the model's performance remains stable across a wide range of parameter values, with only minor variations in the Kappa and Jaccard indices.

The sensitivity analysis also included variations in random seed values, showing that the model produces consistent results across different stochastic realizations, with coefficient of variation less than 2% for all validation metrics.

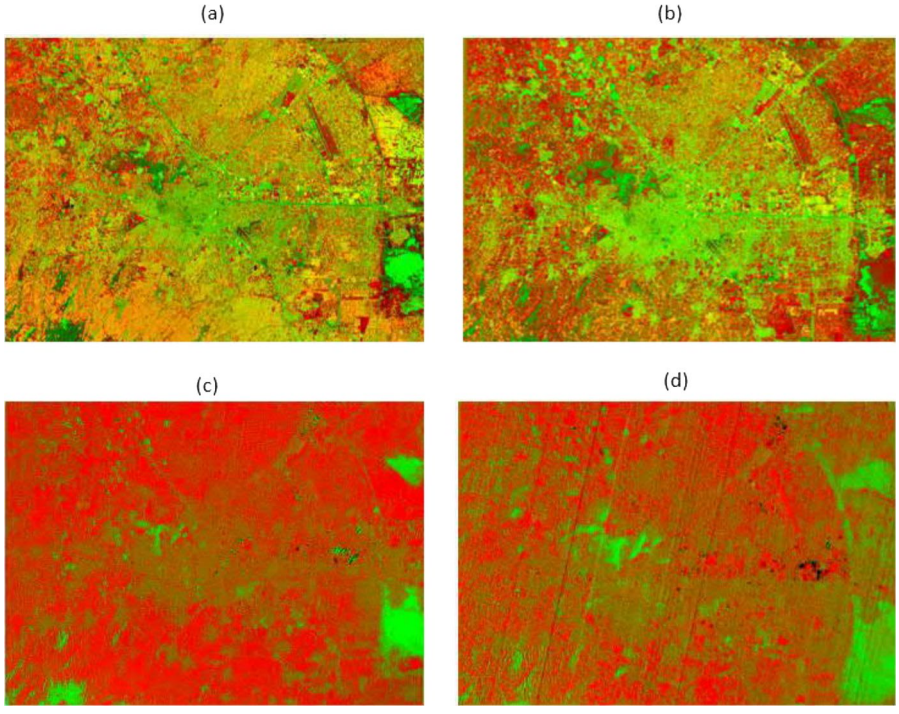

Fig. 8 First and second principal components for Bands 6–7 and 10–11: (**a**) Band 6–7 in 2003; (**b**) Band 6–7 in 2017; (**c**) Band 10–11 in 2003; (**d**) Band 10–11 in 2017.

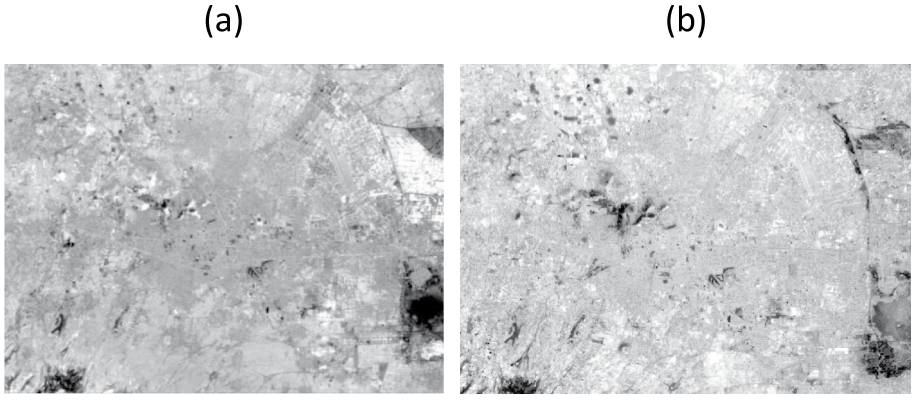

Fig. 9 NDBI index for Toluca: (**a**) year 2003; (**b**) year 2017

This analysis confirms the model's robustness and reliability, ensuring consistent performance even under varying conditions. However, further research is recommended to explore the impact of additional parameters, such as the size of the neighborhood used in the spatial diffusion rules.

4.7 Visual representation of results

To illustrate the methodology and its findings, Figs. 8, 9, and 10 present examples of the analysis for Toluca in 2003 and 2017. Although these images focus on Toluca, they serve as representative examples of the patterns and trends observed across all six cities studied. Figs. 8 and 9 display the first and second principal components and the Normalized

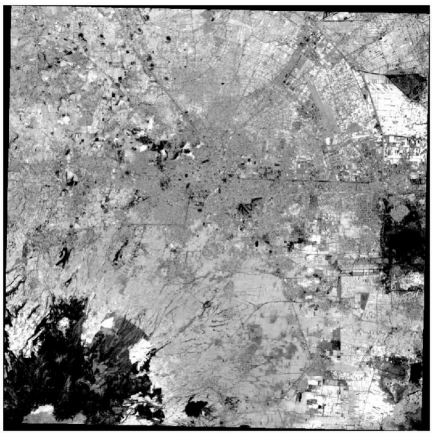

Fig. 10 BAEM output for Toluca, illustrating urban areas

Difference Built-up Index (NDBI), respectively. These visualizations highlight urbanization dynamics during the study period.

In Fig. 8, the principal components for Bands 6–7 and 10–11 show clear differentiation between urban and non-urban areas, whereas in 2003, urban areas in Bands 6–7 exhibit moderate spectral intensity, indicating relatively low urban density (Fig. 8(a) and (c)). By 2017, the intensity increases notably, particularly in Bands 10–11, reflecting the expansion of impervious surfaces and urban sprawl (Fig. 8(b) and (d)).

Figure 9 focuses on the NDBI index, which emphasizes built-up areas. This index is particularly effective in quantifying urban growth: - In 2003, the NDBI values are lower and more scattered, indicating limited urbanization (Fig. 9(a)). - By 2017, NDBI values increase significantly, particularly in the urban core and surrounding regions, confirming the expansion of built-up areas (Fig. 9(b)).

Also, Fig. 10 presents the Built-up Area Extraction Method (BAEM) grayscale output for Toluca. This visualization further supports the analysis by showing a detailed spatial distribution of urban areas: - In 2003, urban regions are concentrated in the city center, with lower intensity values. - By 2017, the grayscale intensity expands outward, reflecting significant urban growth into previously undeveloped areas.

While these figures are specific to Toluca, similar patterns were observed in the other cities studied (Acapulco, Puebla, Querétaro, Tampico, and Tijuana). Urban areas in each city exhibited comparable trends of increased spectral intensity, higher NDBI values, and expanded built-up regions. These findings validate the consistency of the methodology and its ability to capture urbanization dynamics across diverse geographic and socio-economic contexts.

The insights gained from these visualizations are integral to understanding urban expansion as modeled by the Spatial Markov Chain framework. The figures provide concrete examples of how urban growth manifests spatially and spectrally, reinforcing the reliability of the methodology for assessing urbanization in rapidly developing regions.

Figures 11 and 12 illustrate the urban areas of Acapulco, Puebla, Querétaro, Tampico, Tijuana, and Toluca as observed in 2003 and 2017. These images, derived through the binarization process applied to Landsat 8 data, highlight urbanized regions (represented as binary pixels) and provide a clear comparative baseline for analyzing urban expansion trends over time. The binarized format simplifies the identification of urban growth by

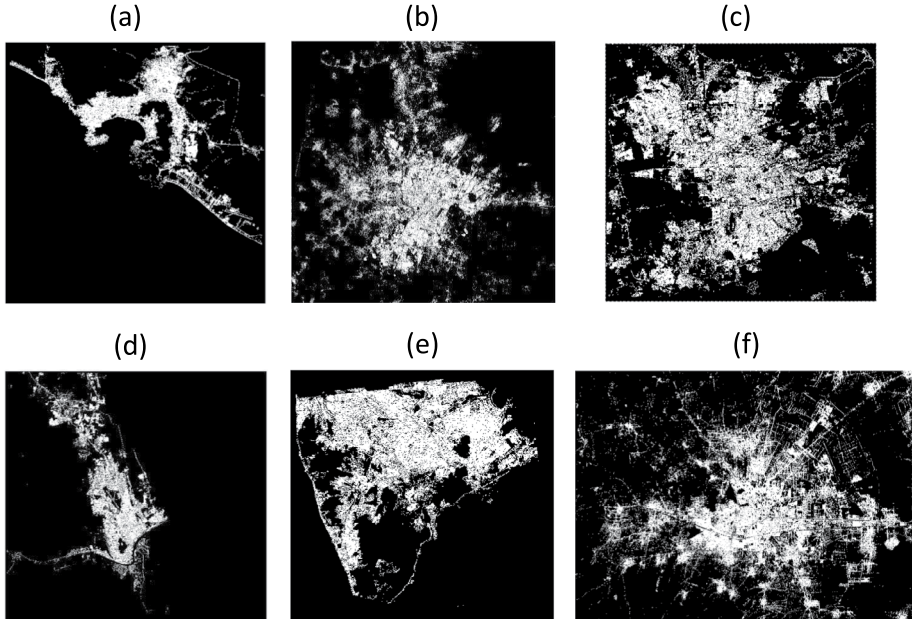

Fig. 11 Urban area distribution for each city in 2003: (**a**) Acapulco, (**b**) Puebla, (**c**) Querétaro, (**d**) Tampico, (**e**) Tijuana, (**f**) Toluca

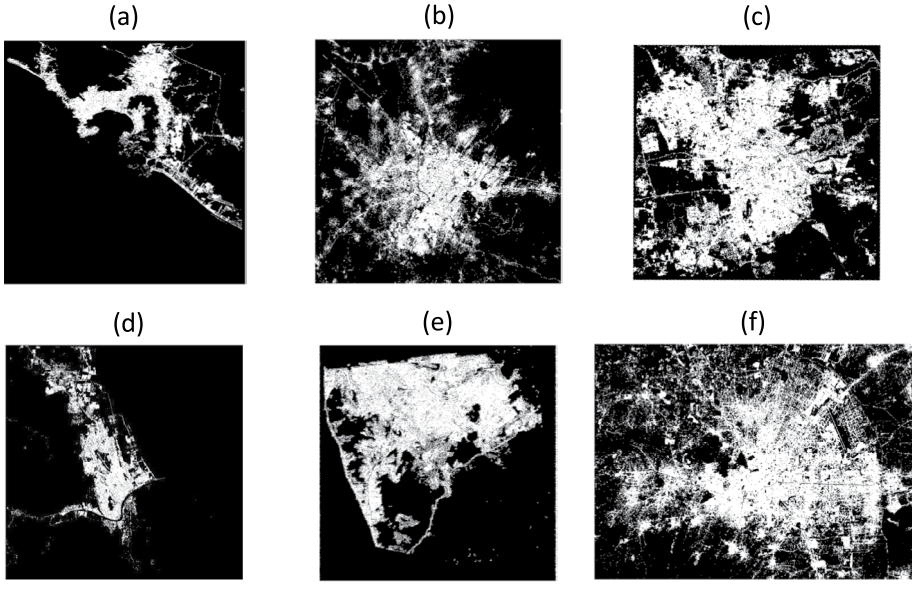

Fig. 12 Urban area distribution for each city in 2017: (**a**) Acapulco, (**b**) Puebla, (**c**) Querétaro, (**d**) Tampico, (**e**) Tijuana, (**f**) Toluca

isolating urban areas from non-urban regions, enhancing the clarity and utility of these visuals for trend analysis.

Using our SMC projections, we extended the urban growth analysis to 2031 (see Fig. 13). The results highlight the model's ability to predict urban expansion while preserving constrained areas, which are expected to maintain their spatial structure over the projection period. These constrained areas include regions with geographic, environmental, or regulatory restrictions that limit urban development, such as protected natural reserves, water bodies, or zones governed by strict urban policies.

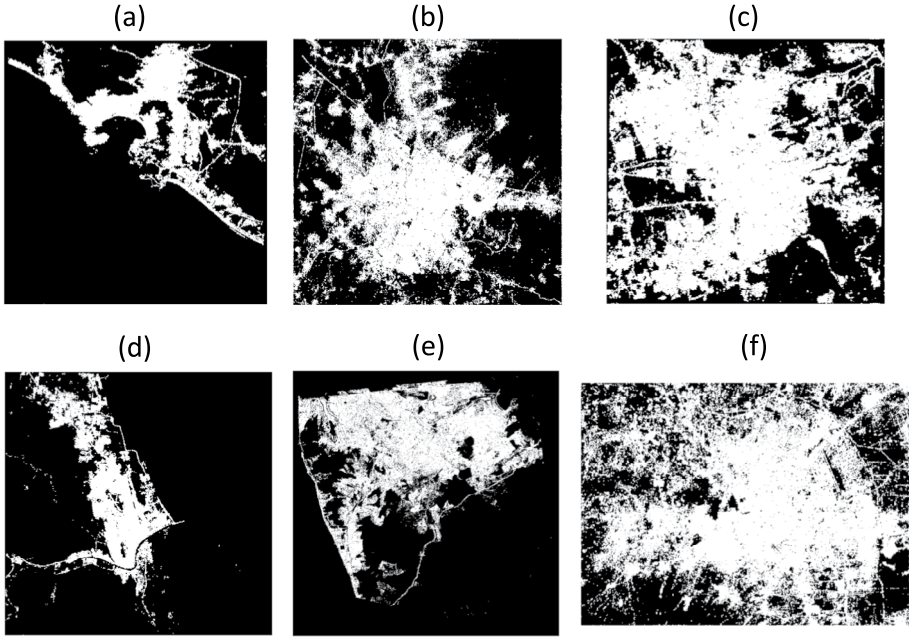

Fig. 13 Projected urban area distribution for each city in 2031: (**a**) Acapulco, (**b**) Puebla, (**c**) Querétaro, (**d**) Tampico, (**e**) Tijuana, (**f**) Toluca

Visual analysis by urban planning experts confirmed the accuracy of the model in retaining these constrained areas, demonstrating its capacity to respect spatial limitations while simulating realistic growth patterns. This validation is particularly significant, as it ensures the model's alignment with expert expectations and urban planning principles, reinforcing its reliability as a tool for decision-making.

The preservation of restricted zones serves not only as a crucial validation criterion but also as an essential aspect of urban planning. It allows planners to forecast urban growth while integrating existing limitations, ensuring that predictions are both reliable and practical. Additionally, pinpointing areas where development is improbable offers critical insights for optimizing resource distribution, advancing infrastructure, and shaping long-term urban strategies. This capability sets the SMC model apart from conventional methods that frequently neglect spatial constraints, thereby increasing its relevance in practical applications.

In summary, the 2031 projections underscore the robustness of the SMC model in simulating urban growth while adhering to known constraints, making it a valuable asset for urban planners seeking to balance expansion with sustainability and regulatory compliance.

5 Discussion

The results of this study demonstrate the effectiveness of the SMC model in projecting urban expansion across diverse geographic and socio-economic contexts. By integrating spatial diffusion rules with probabilistic transitions, the model captures both the temporal dynamics and spatial heterogeneity of urbanization, offering a robust tool for urban planning and policy-making.

5.1 Comparative analysis with existing models

Traditional urban growth models, such as CA-Markov and SLEUTH, have been widely used for land use change projections. However, these models often face limitations in scalability, computational efficiency, and spatial precision. In contrast, the SMC model introduced in this study addresses these challenges by incorporating a semi-automated image processing pipeline and a probabilistic spatial diffusion rule, enabling more accurate and context-sensitive projections.

For instance, CA-Markov models rely on predefined transition rules and neighborhood configurations, which may not fully capture the complex interactions driving urban growth. Similarly, SLEUTH models require extensive calibration and are computationally intensive, limiting their applicability in data-scarce regions. The SMC model overcomes these limitations by leveraging automated image enhancement techniques and adaptive thresholding, reducing the need for manual intervention and enhancing reproducibility.

Moreover, the SMC model's ability to integrate spatial neighborhood effects through diffusion rules provides a significant advantage over classical Markov Chains, which estimate transition probabilities without considering spatial context. This integration ensures that the model not only predicts the likelihood of urban expansion but also allocates it geographically, aligning with observed patterns of urban growth.

When compared with machine learning approaches, the SMC model offers superior interpretability and transparency. While deep learning models may achieve slightly higher accuracy, their black-box nature limits their utility for policy-making where understanding the rationale behind predictions is crucial. The SMC model's probabilistic framework provides clear insights into the factors driving urban expansion, making it more suitable for collaborative planning processes.

5.2 Implications for urban planning

The high accuracy of the SMC model, as validated by metrics such as the Kappa index (0.75–0.81) and Jaccard index (0.68–0.92), underscores its potential as a reliable tool for urban planners. By providing detailed projections of urban expansion, the model can inform strategic decisions related to infrastructure development, environmental conservation, and disaster risk management. For example, identifying areas of high urbanization probability can guide investments in public transportation, water supply, and waste management systems, ensuring that growth is managed sustainably.

Additionally, the model's ability to quantify spatial complexity through entropy and fractal dimension indices offers valuable insights into the environmental impacts of urbanization. Cities with high entropy values, such as Acapulco, may require targeted policies to curb sprawl and promote compact development, while those with low entropy, like Tampico, could benefit from strategies that enhance connectivity and reduce fragmentation.

The model's computational efficiency (approximately 12 minutes per city) makes it particularly valuable for rapid assessment and scenario planning. Municipalities with limited technical capacity can use the model to evaluate multiple development scenarios without requiring specialized hardware or software, democratizing access to advanced urban modeling tools.

5.3 Limitations and future research

Despite its strengths, the SMC model has certain limitations. First, the reliance on moderate-resolution Landsat imagery (30 m/pixel) may limit its ability to capture fine-scale urban features, such as small settlements or informal housing. Future research could explore the integration of high-resolution satellite data or unmanned aerial vehicle (UAV) imagery to enhance spatial detail.

Second, the model currently focuses on biophysical drivers of urban growth, such as land cover and topography, without explicitly incorporating socio-economic variables like population density, income levels, or zoning regulations. Integrating these factors into the transition rules or as additional layers in the diffusion process could improve the model's predictive accuracy and policy relevance.

Third, while the model incorporates basic spatial constraints through exclusion masks, more sophisticated constraint modeling could be implemented using multi-criteria decision analysis (MCDA) techniques. This would allow for finer control over where urbanization is permitted based on environmental sensitivity, infrastructure capacity, and regulatory frameworks.

Finally, while the model demonstrates high computational efficiency for city-scale applications, scaling it to regional or national levels may require optimization for parallel processing or cloud computing environments. Future work could explore these avenues to enhance the model's scalability and accessibility.

5.4 Computational requirements

The SMC model's lightweight architecture requires minimal computational resources compared to alternative approaches. A comparative analysis of computational requirements showed:

- SMC model: 12 minutes per city on standard desktop hardware
- CA-Markov: 18 minutes per city with similar hardware
- MOLUSCE with ANN: 45 minutes per city
- Deep learning models: 2+ hours per city with GPU acceleration

This efficiency makes the SMC model particularly suitable for applications in resource-constrained environments or for rapid assessment of multiple scenarios.

6 Conclusions

This study presents a semi-automated Spatial Markov Chain (SMC) model for projecting urban expansion, integrating automated image processing with probabilistic spatial diffusion rules. The model was applied to six major Mexican cities, demonstrating its ability to capture both the magnitude and spatial patterns of urbanization with high accuracy. Validation metrics, including the Kappa index, Jaccard index, Shannon entropy, and fractal dimension, confirm the model's robustness and reliability.

The SMC model offers several advantages over traditional urban growth models, including scalability, computational efficiency, and spatial precision. By providing detailed projections of urban expansion, it serves as a valuable tool for urban planners and policymakers, supporting sustainable development and informed decision-making.

The key methodological innovations of this research include:

1. A semi-automated framework that balances accuracy with computational efficiency

2. Integration of spatial diffusion rules with probabilistic transitions
3. Application of exclusion masks to respect geographical constraints
4. Validation using multiple temporal points and comparative benchmarks

These innovations address critical gaps in existing urban modeling approaches, particularly the trade-off between sophistication and accessibility.

Future research directions include the integration of high-resolution imagery, socio-economic variables, and machine learning techniques to further enhance the model's predictive capabilities. By addressing these aspects, the SMC framework can evolve into a comprehensive tool for managing the complex challenges of urbanization in the 21 st century.

Author contributions
All authors contributed equally to this work

Funding
This work received no funding.

Data availability
The data supporting the findings of this study are available from the corresponding author upon reasonable request.

Declarations

Ethics approval and consent to participate
Not applicable.

Consent for publication
Not applicable.

Competing interests
The authors declare no competing interests.

Received: 3 July 2025 / Accepted: 17 November 2025
Published online: 09 December 2025

References

1. Ambrosio G, González J, Arévalo V. Corrección radiométrica y geométrica de imágenes para la detección de cambios en una serie temporal (2002)
2. Ariza A. Descripción y corrección de productos landsat 8 ldcm (landsat data continuity mission). Technical report, Centro de Investigación y Desarrollo en Información Geográfica del IGAC - CIAF (2013)
3. Bhatti SS, Tripathi NK. Built-up area extraction using landsat 8 oli imagery. GIScience & Remote Sensing. 2014;51:445–67.
4. Chen J, Gong P, He C. Recent advances in land-use/land-cover change detection. Remote Sens Lett. 2023;14(3):456–78.
5. Clarke KC, Johnson JM. Calibrating sleuth with big data: projecting California's land use to 2100. Comput Environ Urban Syst. 2020;83:101525.
6. Congalton RG. Advances in assessing the accuracy of classifications of remotely sensed data. J Remote Sens. 2022;12(4):305–15.
7. Ezimand K, Aghighi H, Ashourloo D, Shakiba A. The analysis of the spatio-temporal changes and prediction of built-up lands and urban heat islands using multi-temporal satellite imagery. Sustain Cities Soc. 2024;103:105231.
8. Espinoza JCP. Satellite image analysis for heavy metal monitoring in mining sites. Remote Sensing Applications. 2022;10(2):102–17.
9. Gómez PA, Sánchez LT. Spatial markov chains for urban growth simulation: Toluca metropolitan area 2023–2035. Urban Stud. 2023;60(7):1203–30.
10. Herrera AMM. Random numbers: modern applications and theoretical insights. Int J Comput Methods. 2021;18(2):345–69.
11. Han-Qiu X. Enhanced water body information extraction using advanced MNDWI. Remote Sensing Journal. 2021;15(3):789–801.
12. He Y, Wu W, Xie X, Ke X, Song Y, Zhou C, et al. Land use/cover change prediction based on a new hybrid logistic-multicriteria evaluation-cellular automata-markov model taking hefei, China as an example. Land. 2023;12(10):1899.
13. Irwin EG, Geoghegan J. Theory, data, methods: developing spatially explicit economic models of land use change. Agric Ecosyst Environ. 2001;85(1–3):7–24.
14. Jardon E, Jiménez E, Romero M. Spatial markov chains implemented in gis. In: 2018 International Conference on Computational Science and Computational Intelligence (CSCI). 2018;1:361–367.
15. Jardon E, Romero M. Descripción, combinación y tratamiento de imágenes ráster obtenidas del satélite landsat 8. Komputer Sapiens. 2019;6–10.
16. Khargonekar PP, Samad T. The United Nations sustainable development goals: an IFAC agenda. IFAC-PapersOnLine. 2024;58(3):153–8.

17. Kushwaha K, Singh M, Singh SK, Patel A. Urban growth modeling using earth observation datasets, cellular automata-markov chain model and urban metrics to measure urban footprints. Remote Sensing Applications Society and Environment. 2021;22:100479.
18. Li M, Cao Y, Dai J, Song J, Liang M. A comprehensive review of urban expansion and its driving factors. Land. 2025;14(8):1534.
19. Lee C. New models for urban planning in a digital era. Plan Rev. 2020;38(4):215–39.
20. López E, Mendoza M, Acosta A. Land-use change in endorheic basins: a case study of lake cuitzeo, Michoacán. Journal of Ecological Studies. 2021;78(5):45–62.
21. López AM.: Introduction to Artificial Life and Cellular Automata (2020). http://uncomp.uwe.ac.uk/genaro/new_version/artificial_life.pdf
22. Martínez AR, Hernández PL. Migration dynamics and socioeconomic factors influencing municipal attractiveness in mexico, 2010–2030. J Migr Reg Stud. 2023;31(4):320–45.
23. NASA: New Tool Provides Rapid Evaluation of Water Quality. Consulted on 23/06/2025 (2024). https://landsat.gsfc.nasa.gov/article/new-tool-provides-rapid-evaluation-of-water-quality/
24. Nouri J, Gharagozlou A, Arjmandi R, Faryadi S, Adl M. Predicting urban land use changes using a ca-markov model. Arab J Sci Eng. 2014;39:5565–73.
25. Ogashawara I, Bastos V. Urban heat islands and land cover: a quantitative analysis. J Urban Remote Sens. 2023;18(1):67–89.
26. Rosa VP, Benavente FA, Rocha WP. et al. Urban growth simulation models: A comparative study. In: National Conference on Geospatial Information Technologies, University of Seville. 2021;134–145.
27. Reyes PR, Torres-Florez JP. Deep-water chondrichthyans diversity in the patagonian archipelago. Mar Biol Oceanogr Rev. 2021;17(4):145–65.
28. Subedi P, Subedi K, Thapa B. Application of a hybrid cellular automaton-markov (ca-markov) model in land-use change prediction: a case study of saddle creek drainage basin, florida. Appl Ecol Environ Sci. 2013;1(6):126–32.
29. Team QD.: MOLUSCE: Modules for Land Use Change Evaluation. https://plugins.qgis.org/plugins/molusce/
30. Tomasi C, Kanade T. Advances in point feature detection and tracking. Computer Vision Technical Reports (2023)
31. USGS: Update of Landsat: Special issue 2023. Consulted on 23/06/2025 (2013). https://www.usgs.gov/landsat-missions
32. Vafeidis AT, Koukoulas S, Gatsis I, Gkoltsiou K. Forecasting land-use changes with the use of neural networks and gis. In: 2007 IEEE International Geoscience and Remote Sensing Symposium. 2007;5068–71.
33. Wu P, Zhang Z, Peng X, Wang R. Deep learning solutions for smart city challenges in urban development. Sci Rep. 2024;14(1):5176.